HHS Public Access

Author manuscript

Neuroendocrinology. Author manuscript; available in PMC 2017 January 01.

Published in final edited form as:

Neuroendocrinology. 2016 ; 103(6): 650–664. doi:10.1159/000442015.

Age and Long-Term Hormone Treatment Effects on the Ultrastructural Morphology of the Median Eminence of Female Rhesus Macaques

Michelle M. Naugle[1], **Sateria A. Lozano**[2], **Fay A. Guarraci**[5], **Larry F. Lindsey**[3], **Ji E. Kim**[2], **John H. Morrison**[6], **William G.M. Janssen**[6], **Weiling Yin**[2], and **Andrea C. Gore**[1,2,4,*]

[1]Institute for Neuroscience, University of Texas at Austin, Austin, TX

[2]Division of Pharmacology & Toxicology, University of Texas at Austin, Austin, TX

[3]Center for Learning and Memory, University of Texas at Austin, Austin, TX

[4]Institute for Cellular & Molecular Biology, University of Texas at Austin, Austin, TX

[5]Department of Psychology, Southwestern University, Georgetown, TX

[6]Fishberg Department of Neuroscience and the Friedman Brain Institute, Icahn School of Medicine at Mount Sinai, New York, NY

Abstract

The median eminence (ME) of the hypothalamus comprises the hypothalamic nerve terminals, glia (especially tanycytes) and the portal capillary vasculature that transports hypothalamic neurohormones to the anterior pituitary gland. The ultrastructure of the ME is dynamically regulated by hormones and undergoes organizational changes during development and reproductive cycles in adult females, but relatively little is known about the ME during aging, especially in non-human primates. Therefore, we used a novel transmission scanning electron microscopy (tSEM) technique to examine the cytoarchitecture of the ME of young and aged female rhesus macaques in a preclinical monkey model of menopausal hormone treatments. Rhesus macaques were ovariectomized and treated for 2 years with vehicle, estradiol, or estradiol + progesterone (E_2 + P_4). While the overall cytoarchitecture of the ME underwent relatively few changes with age and hormones, changes to some features of neural and glial components near the portal capillaries were observed. Specifically, large neuroterminal size was greater in aged compared to young adult animals, an effect that was mitigated or reversed by E_2 alone but not E_2 + P_4 treatment. Overall glial size, and the density and tissue fraction of the largest subset of glia, were greater in aged monkeys, and in some cases reversed by E_2 treatment. Mitochondrial size was decreased by E_2, but not E_2 + P_4, only in aged macaques. These results contrast substantially with work in rodents, suggesting that the ME of aging macaques is less vulnerable to age-related disorganization, and that estradiol's effects in the monkey ME are age-specific.

*Correspondence: Andrea C Gore, PhD, The University of Texas at Austin, 107 West Dean Keeton, C0875, Austin, TX, 78712, USA, andrea.gore@austin.utexas.edu; Tel: +1-512-471-3669; Fax: +1-512-471-5002.

Disclosure Statement: The authors have nothing to disclose.

Keywords

Aging; Monkey; Estradiol; Progesterone; Median Eminence; Glia; Mitochondria; Hypothalamus

Introduction

Menopause is a natural transition occurring in all women at midlife, and is heralded by a decline in estradiol (E_2) and progesterone (P_4) production, and the cessation of menstrual cycles. The menopausal transition is often accompanied by neurobiological symptoms such as vasomotor symptoms, sleep and mood disruptions, and cognitive changes, presumably due to the relatively abrupt deprivation of ovarian E_2 and P_4; these can have a dramatic impact on quality of life [1–5]. Hormone replacement therapies (HRT) with E_2 alone (in hysterectomized women) or in combination with P_4 (for women with a uterus) are used primarily to improve vasomotor symptoms, vaginal dryness, and osteoporosis, and while not used specifically for other neurobiological symptoms, also exert actions on these latter endpoints [6, 7].

Within the hypothalamus, the median eminence (ME) is a circumventricular structure that allows communication between the brain's ventricular system, neurons, glia, and the portal vasculature leading to the anterior pituitary gland [8–11]. In the ME, the hypophysiotropic neuroterminals that arise from nerve terminals of releasing- and inhibiting-hormones release their contents into the extracellular space that adjoins the portal capillary bed that vascularizes the adenohypophysis [9, 12–14]. Within the hypophysiotropic nerve terminals, peptide hormones are packed into large dense core vesicles (LDCV) where they are available for release into the pericapillary region of the ME for release [15–19]. Tanycytes, specialized astrocytes in the ME, are particularly important to the regulation of the endocrine system because their motile processes wrap around the hypophysiotropic neuroterminals and guide them to the capillary, and tanycytic endfeet form part of the blood-brain-barrier; therefore they act as a 'gatekeeper' for hypothalamic hormonal release [10, 11, 18, 20–26].

The role of the ME in reproductive aging is an important but understudied research area, particularly because of the high estrogen sensitivity of this region and the ability of E_2 to induce dynamic morphological changes to nerve terminals and glia [11, 19, 25–28]. Previously, our lab reported striking changes in the morphological organization and cytoarchitecture of the ME of aging rats, but little effect of short-term E_2 treatment [16, 17]. In monkeys, age- and E_2-related changes were found in expression of genes encoding for kisspeptin, neurokinin B and prodynorphin (*KISS1, NKB* and *PDYN)* in a dissection containing the combined arcuate nucleus plus ME [28]. Recently, we demonstrated that GnRH nerve terminals in the ME of aging monkeys co-express the membrane estrogen receptor, G protein-coupled estrogen receptor (GPER), and form close appositions with GPER-positive processes, but found little evidence for age- or long-term E_2, with or without P_4 treatment effects [29]. Given this relative dearth of information on the aging ME in monkeys, and in light of known differences in reproductive senescence between rats and nonhuman primates [30–33], we took advantage of the availability of a recently-developed new electron microscopic technique to examine the ultrastructure and cytoarchitectural

properties of the ME, and the relationship between glia and neuroterminals, in young and aged female rhesus macaques given a clinically-relevant model of HRT.

Methods

Animals

Female monkeys (*Macaca mulatta*) that were young premenopausal adults (n = 18, 9.8 ± 2.2 years), or aged peri- or post-menopausal adults (n = 18, 22.7 ± 1.6 years) were used in this study. Reproductive status was determined by daily visual inspection of vaginal bleeding, and animals with cycle lengths between 24 to 34 days were included in the premenopausal group [34, 35]. Housing and experimental conditions at the California National Primate Research Center were described previously [36–40]. All procedures were in compliance with the National Institutes of Health Guide for the Care and Use of Laboratory Animals and approved by the Institutional Animal Care and Use Committee at the University of California.

Ovariectomy & Hormone Treatment

The monkeys were ovariectomized (OVX) as described previously [36–41] using isoflurane anesthesia and atropine (0.4 mg/kg) and ketamine (10 mg/kg) sedatives. After 2–3 months of recovery, the young (Y) and aged (A) animals were assigned to one of three groups: estradiol (YE, AE), estradiol plus progesterone (YEP, AEP) or a blank vehicle (YV, AV) treatment. To achieve a mean serum level of ~150 pg/ml, Silastic capsules (0.46 inner diameter and 3 cm long) containing either crystalline estradiol (E_2, Sigma) or empty (for vehicle group) were implanted between the shoulder blades and replaced every three months. To mimic luteal phase P_4 levels, the YEP and AEP groups received micronized progesterone (100 mg; Catalent Pharm Solutions) in their daily fruit treat for 10 consecutive days once per month. Serum concentrations and assay characteristics of E_2 were previously reported for this cohort of young [42] and aged monkeys [43]. For the young YV, YE, and YEP groups at perfusion, serum E_2 concentrations (mean ± SEM, pg/ml) were 2.0 ± 2.2, 109 ± 15, and 118 ± 13, respectively. For the aged AV, AE, and AEP groups at perfusion, concentrations of E_2 (pg/ml) were 14.9 ± 2.3, 152 ± 41, and 148 ± 17, respectively, confirming that targeted E_2 concentrations were achieved. Six to eight animals were originally included in these groups, but there was attrition due to illness, death, or incomplete OVX, determined by hormone analysis at the time of euthanasia. Additionally, due to the fragility of the tissue and loss during the cryopreparation process, final group numbers for electron microscopy were: YV n=4, YE n=5, YEP n=4, AV n=4, AE n=4, AEP n=4. As described previously [43, 44], the monkeys were euthanized 8–10 days after the last P_4 treatment or the corresponding day for no P_4 groups, after an average of two years of hormone treatment.

Euthanasia & Tissue Preparation

The animals were deeply anesthetized with pentobarbital (20–35 mg/kg) and ketamine (25 mg/kg) and were transcardially perfused with ice-cold paraformaldehyde (PFA) in 0.1 M phosphate buffer (PB), using 1% PFA for 1 minute and increasing the concentration to 4% PFA for 12 minutes, with the flow rate set to 185 ml/min. The brain was removed and the

hypothalamus was post-fixed in 0.125% gluteraldehyde and 4% PFA for 6 hours, then shipped, on ice, to the University of Texas at Austin in PB.

Using a vibrating microtome (Leica VT1000 S; Leica, Bannockburn, IL), we collected 10–25 coronal sections at 100 μm, through the entire ME region, when present. Sections were cryoprotected via immersion in a series of increasing concentrations of glycerol in 0.1M PB: 10% 1 hour, 20% 1 hour, and 30% twice for an hour and then overnight, all with constant agitation. Eight of these sections, in a rostral to caudal series, were selected for electron microscopy (EM) analysis. The dorsal-most portion of the ME was dissected and embedded in a Lowicryl resin block using cryofixation system (Leica CPC, Vienna) with an automatic freeze-substitution unit (AFS; Leica AFS, Vienna) as previously described [36, 39, 45, 46] and modified from [47–49]. Briefly, each 100 μm blocks was mounted on the head of a pin and rapidly plunged into liquid propane that was cooled to −190°C. The specimens were rapidly transferred to the AFS apparatus that was pre-cooled to −90°C for Lowicryl freeze substitution. The tissue was immersed in 1.5% uranyl acetate in anhydrous methanol for 24 hours, the temperature was increased by 4°C every hour to −45°C, then rinsed in anhydrous methanol and infiltrated with Lowicryl resin HM20 (Electron Microscopy Sciences, Ft. Washington, PA) with a four-step series of increasing concentration of resin to methanol (doubled each time; 1 hour each) and then in 100% Lowicryl for 12 hours. The resin was polymerized by ultraviolet light (360 nm) for 48 hours at −45°C, then 24 hours at room temperature and the resulting blocks were prepared for ultrathin sectioning. The remaining 100 μm ME sections were retained for immunofluorescence analysis [29].

We collected sections for EM imaging using an ultramicrotome (Leica EM UC6, Vienna), positioned on a floating table and surrounded by a Plexiglas enclosure. The block face was trimmed to expose the ME sample with a glass knife and we collected 400 nm semi-thin sections for identification of the boundary between the portal capillary bed and the dorsolateral portion of the ME block. The semi-thin sections were mounted on glass slides, dried on a hotplate for 10 minutes at 100°C, stained with 2% toluidine blue and examined with a bench-top transmitted light microscope (Leica DMLB upright microscope, Germany). After determining where to start cutting ultrathin sections, five to ten 70 nm consecutive sections were cut with a 45° ultra diamond knife (Diatome, Hatfield, PA), collected on separate formvar-coated gold slot grids (Electron Microscopy Sciences, Fort Washington, PA). A flow chart of the tissue processing and imaging is shown in Figure 1.

Transmission-mode scanning electron microscopy (tSEM)

The images of the ultrathin sections were captured using tSEM, a newly developed system that consists of a field-emission scanning electron microscope (Zeiss supra 40VP FE-SEM) fitted with a retractable transmitted electron detector, a 12-grid specimen holder and integrated with the Zeiss ATLAS™ [50, 51]. Unlike conventional transmission electron microscopes (TEM), this system uses low electron doses that reduce physical and optical distortion and leaves the specimen intact for analysis. Additionally, the 12-grid specimen holder and semi-automated ATLAS™ system, dramatically reduced the time and labor involved in image collection. We took multiple large field, high resolution images along the basal lamina that separates neural tissue from the portal capillary bed of each animal [16];

field-size = 25,000 × 25,000 pixels @ 2 nm^2 pixel size), which allowed us to collect all of our sample sites from an individual monkey in a single imaging session. We then randomly selected 9–10 sites abutting capillaries on the distal edge of the ME (10,000 × 10,000 nm) for analysis. When we could not find enough sites on a single section, we imaged a second section that was at least 500 nm apart from the previous site to prevent resampling the same region. Within each of these 9–10 sites, we chose a 5,000 × 5,000 nm field that contained at least one neuroterminal with large dense-core vesicles for further analysis. All sampling sites were separated by a minimum of 5,000 nm to prevent re-sampling the same structures.

tSEM Image Analysis

Analysis was performed to quantify the size, density, and ME tissue fraction of nerve terminals, glia, mitochondria, and extracellular space within 5 μm of a capillary for each monkey. We also determined the percent of glia and neuroterminals in contact with the capillary. We used TrakEM2, a plugin for Fiji, freely available NIH-sponsored image analysis software, for manual image segmentation [52]. The membrane boundaries of all identifiable neuroterminals, glia, mitochondria and basal lamina were traced and filled in with a unique color representing the class of the object (red, green, blue, and magenta, respectively) on 9–10 capillary sites in 1–2 sections. Neuroterminals were distinguished from glia by the presence of large dense-core vesicles (LDCV), small clear vesicles and/or neurofillaments and mitochondria were identified by their cristae [53]. In an attempt to isolate the physiologically relevant components, we separated the cellular components into three size-based categories: the smallest category (0.01–0.2 μm^2) contained only cross sections of cellular processes (0.01 μm is the mean cross section area of mitochondria and the lower limit of our ability for identification), the medium category (0.2–1.0 μm^2) contained some length-wise cross-sections of cellular processes and some smaller neuroterminals and endfeet of glia, and the largest category (> 1.0 μm^2) contained only secretory neuroterminals and globular endfeet of glia.

To determine area, density, and class of the segmented components, a second set of images was produced, identical to the first, but with the mitochondria removed. A custom Matlab program (R2013b, Mathworks) was designed to analyze the differences between the image pairs, as follows (Figure 1): for each image pair, a binary (black or white) image, or mask, was created for each type of region by color comparison against the first image in the pair. This mask was composed of several connected components, each representing a single cross section. We used connected component analysis to extract information about the number of components and the number of pixels that are contained in each. Similarly, we found a mask for mitochondria in the second image by searching for blue pixels. By taking the pixel-wise AND-operation between the mask corresponding to terminals or glia, and the one corresponding to mitochondria, we were able to determine the cell type to which each mitochondria corresponded, as well as the size and count for these organelles. The software compiled the information in these images into object count, average object size, and the fraction of non-capillary pixels occupied by terminals, glia, and mitochondria and also categorized each mitochondria as belonging to a terminal or glial. We also used custom software written in Python (v3.4.3 www.python.org) to quantify the relative length of glia and neuroterminal contacts with capillaries for each animal. The program measures the

length by computing a binary “mask” for each image, representing the capillary, glia, and neuroterminal bodies. The capillary mask was dilated by 50 nm. The intersection of this new mask with the masks of the glia and neuroterminals was then taken. Where such an intersection existed, its skeleton was computed, and then measured for length. The skeletonization algorithm we used is available as part of the popular open source scikit-image library. This code is available at https://github.com/larrylindsey/NaugleEtAl2015/tree/Neuroendocrinology

Immunofluorescence and confocal microscopy of GnRH

Immunoflorescence and confocal microscopy were used to analyze the density of GnRH positive neuroterminals in the monkey ME, as described previously [54]. We had published a colocalization analysis of double-labeling of GnRH and GPER signaling in GnRH cell bodies and terminals [29], on tissues collected from the same cohort of monkeys. The confocal results of the GnRH signals in the ME were not previously published, so we used that available dataset to estimate the density of GnRH terminals in the external zone of the ME from 1–2 100 μm sections per monkey. Immunohistochemistry (IHC) of GnRH was described in [29], using the mouse monoclonal anti-GnRH primary antibody (HU11b, diluted to 1:1,000; a gift from Dr Henryk Urbanski; [55]) followed by incubation in the secondary antibody [Alexa Fluor 594 conjugated goat anti-mouse IgG (diluted 1:400; Life Technologies, Eugene, OR, USA)]. We also note that we attempted to perform direct IHC of GnRH in the samples prepared for tSEM, but were unable to obtain successful specific labeling, presumably due to loss of antigenicity in the samples during tissue preparation, as the IHC method worked in other tissue types.

To determine the density of GnRH immunofluorescent neuroterminals in the ME, we examined the external zone of the ME sections for each animal. From the surface of each tissue section, a stack of 10 images (in a 6.6 μm thickness) was captured using a Zeiss LSM 710 confocal microscope, Zen Black software (Carl Zeiss International, version date: 2012) with a Plan-Apochromat 40x/1.4 Oil DIC M27 objective. The laser power, gain and offset were set such that there was no signal visible in the negative control section. To decrease background and prevent signal bleed-through we took the average of two scans for each line in the image. We used an excitation wavelength 561 nm (detection range 566 nm – 689 nm). Immunofluorescent signals were observed as strings of punctate labels more concentrated in the external zone of the ME.

Confocal Image Analysis

For stereologic quantification, a physical disector method [54] was used to quantify the density of GnRH puncta in a 106 μm by 106 μm by 6.6 μm volume in the external zone of the ME. This method compares objects in two images, and counts only the objects that were observable in the first section (reference section) but not in the adjacent section to avoid double counts. Five pairs of images from each animal were processed using NIH imaging software Image J 2.0.0-rc-32/1.49v (http://fiji.sc/Fiji). In each pair of images, the reference image and adjacent image were 0.66 μm apart. The images were thresholded and binarized to highlight GnRH puncta. The number of terminals in each image was quantified using the ‘analyze particles’ command. Using the Z Project function, particles representing the puncta

that appeared in both reference and adjacent images were separated by threshold. Puncta detected as particles from the project image were then quantified. The density of GnRH puncta was estimated as [(# particles in reference image – # particles in project image)/ volume]. It should be noted that fluorescence signal might decrease from the surface into the tissue depth; therefore it is possible that using a reference image close to the surface could lead to an overestimate of density. To adjust for this, we used the average density calculated from both directions in a pair of images.

Statistical Analysis

We used R for all statistical analysis (R Development Core Team, 2012). Our dataset failed the assumptions required for ANOVA, as determined by Levene's equality of variance and the Shapiro-Wilks normality tests, therefore we used the Kruskal-Wallis non-parametric test to determine significant main effects of age, treatment, or interactions ($p < 0.05$), followed by the pairwise Wilcoxon rank sum post-hoc test when indicated by a significant main effect.

Results

Ultrastructure of the ME

Figure 2 shows a tSEM image of a representative AV monkey, illustrating the segmentation process and identification of intracellular components. The pericapillary region of the ME contained many neuroterminals that included large dense-core vesicles as well as small clear vesicles and mitochondria, and these terminals were in close apposition with glia, as shown in representative images from four animal in each group (Figure 3).

Age and hormone effects on neuroterminals

Effects of age and hormone treatment were analyzed for neuroterminal size, density, and the tissue fraction (%) in large (> 1.0 μm^2), medium (0.2–1.0 μm^2), and small (0.01–0.2 μm^2), nerve terminals in the ME, as well as for all neuroterminals combined. The size of large terminals in aged animals was significantly greater than in the young monkeys ($p<0.01$), and there was an interaction of age and treatment such that E_2 treatment mitigated this age-related increase in the aged group (Figure 4). There were no age, treatment or interaction effects on these features in medium or small terminals, and no effect when all terminals were combined (Figure 4). Neuroterminal density showed no significant age, treatment or interaction effects in any size category (Figure 4). For tissue fraction, there was a significant effect of treatment ($p<0.05$) on the percent of tissue occupied by large neuroterminals, with E_2 treatment decreasing the tissue fraction in both age groups (Figure 4). The distribution pattern of neuroterminal size is shown in Figure 5A.

Age and hormone effects on glia

A significant difference was found in the size of all glia, which were greater in the aged than the young animals ($p<0.05$; Figure 6). When subdivided into large, medium, or small glia, no significant effects were detected in any of the subcategories. The density of large glia was significantly greater in aged than in young monkeys ($p<0.05$), and there was no effect of age or treatment on the density of all, medium, or small glia (Figure 6). For tissue fraction, there

were significant age effects and an interaction of age with hormone on the percent of tissue containing large glia ($p<0.05$ for both). Post hoc analysis revealed that a greater tissue fraction was covered by large glia in the AV group compared to both the AE and the YV groups (Figure 6). The distribution pattern of glial size is shown in Figure 5B.

Hormone treatments affect mitochondria size in terminals and glia

There was a main treatment effect, and a significant age by treatment effect on the size of all mitochondria ($p<0.05$; Figure 7), driven by the AE monkeys having smaller sized mitochondria compared to the AV and AEP monkeys ($p<0.05$ for both). Within neuroterminals, a significant treatment effect ($p<0.05$) and an interaction of age and treatment ($p<0.05$) was found for mitochondrial size, with AE monkeys again having smaller mitochondria than the AV monkeys. In the glia, mitochondrial size was affected by treatment, and age by treatment interactions were also found, due to the AE monkeys having smaller glial mitochondria than the AV and the AEP groups ($p<0.05$ for both). There were no effects of age, treatment, or interactions on mitochondrial density or on the tissue fraction of mitochondria (Figure 7). The distribution pattern of mitochondrial size is shown in Figure 8.

Hormone treatments do not affect GnRH immunofluorescence density in aged animals

The density of GnRH immunoreactive puncta as analyzed by confocal microscopy in the external ME (Figure 9) was not significantly affected by age or treatment, although there was a trend for a treatment effect ($p = 0.097$) attributable to the $E_2 + P_4$ groups having a non-significantly higher density compared to the vehicle or E_2-alone groups. No interactions of age or treatment were detected.

Capillary contacts with terminals and glia, and extracellular space, are not affected by age or treatment

Effects of age and hormone treatment were analyzed for the interface of the capillaries with glial and terminal components (Figure 10). In all groups, about 40–60% of the capillary was in contact with glia and 12–24% was in contact with terminals. There were no significant differences between age or treatment groups. About 15–30% of the ME was represented by extracellular space (data not shown). There were no significant effects of age, treatment or interactions on the percent of extracellular space, although there was trend for an age effect, with a higher percent of extracellular space in young than aged animals ($p = 0.09$).

Discussion

In the current study, we used transmission Scanning Electron Microscopy (tSEM) to perform both qualitative and quantitative assessments of ultrastructural properties of the pericapillary region of the ME of female rhesus monkeys in a model of menopause. This provides an important methodological advance over previous EM methodologies due to decreased image and tissue distortion and rapid capture of high-resolution large field images [50, 51]. We also used immunofluorescence and confocal microscopy to quantify the density of GnRH puncta in the same region. We applied these methods to address the question of how age and long-

term hormone deprivation or replacement affected these characteristics in a non-human primate.

Because the morphological plasticity of the ME is critical for normal functioning of the neuroendocrine systems, we focused our analyses on ultrastructural properties of neurosecretory terminals and glia [11, 14, 25, 26]. Wholesale cytoarchitectural changes were not observed in our study, but this is not surprising based on evidence that the aging brain often undergoes subtle but functionally-relevant phenotypic changes. For example, effects of age and/or hormone treatment were assessed in female rhesus monkeys for their effects on cognitive function, and these animals' brains utilized for morphometric analyses of prefrontal cortex and hippocampus. When comparing young (~10 year) and aged (~30 year) intact female monkeys on performance on the delayed non-matching to sample (DNMS) test of visual recognition memory, there was an age-related deficit in memory, together with a decrease in density of GluA2 labels (immunogold particles) in the dentate gyrus outer molecular layer dendric spines [56]. Other morphometric endpoints such as dendritic spines, perforated synapse spines, and postdynaptic density were unaffected by age, underscoring the specificity of age-related changes to a subset of measures, and their relationship to a behavioral outcome. Another study utilized young intact monkeys (~10 years) and aged (~22 years) OVX monkeys given injections of vehicle or E_2-cypionate every 3 weeks for 2–3 years [39]. Aged OVX monkeys performed worst on the working memory tasks, and had changes in the subset of donut-shaped mitochondria, both of which were reversed in the E_2 group.

In the current study on the ME, our major results were that the pool of large neuroterminals underwent an age-related increase in size, an effect that was reversed in the E_2 group. In both ages, the tissue fraction represented by these largest nerve terminals was also decreased in the E_2 compared to the vehicle groups at both ages, but not in the $E_2 + P_4$ groups, suggesting that P_4 reversed the E_2 effect. Regarding glia, again it was the pool of largest glia that were affected, as density and tissue fraction of large glia was higher in the aged monkeys, and for tissue fraction, was decreased in the aging monkeys by E_2 treatment. Finally, while there were no age effects on properties of mitochondria, E_2 decreased mitochondrial size only in aged monkeys. It is interesting that in general, the directionality of change was an age-related increase in size, density, and/or tissue fraction; and that E2 reversed some of these effects, mainly in the aged monkeys. Together these results suggest that specific aspects of the ultrastructure of the ME change with age in primates and that long-term HRT can mitigate some of these changes.

Ultrastructure of the ME

The ME is organized into an internal zone, which surrounds the base of the third ventricle and the cell body of tanycytes, and an external zone that contains a high density of glial support cells such as astrocytes, microglia and tanycyte projections [14, 24, 57]. Tanycytes are particularly important to the regulation of the endocrine system because their endfeet act as the gatekeeper to the portal capillary system by blocking or permitting vesicle release under different physiological conditions [18, 20, 21]. Therefore, for our analyses, we sampled and analyzed areas that included one or more neuroterminal possessing LDCVs,

often containing small clear vesicles and mitochondria and in close apposition to glia [58, 59]. We found that the general organization of the rhesus ME is qualitatively different from the rodent in both young and aged adults. In our monkeys, the basal lamina was very convoluted in both young and aged adults and we did not notice any obvious age- or hormone-related differences. By contrast, the ME of young rats is much more highly organized, with little convolution of the basal lamina [16, 17, 60]. Additionally, the linear organization of tanycytic projections from the third ventricle to the capillary bed seen in rodents [16, 17, 24] was not obvious in monkeys of either age.

Age and hormone effects on neuroterminals and glia

We observed a significant increase in the size of large neuroterminals near the capillaries of our aged animals. With respect to hypothalamic-pituitary-gonadal regulation, in monkeys and humans, gonadotropin-releasing hormone (GnRH) release increases with age, and our observed increased terminal size may accommodate larger numbers of LDCV that are waiting to be released, consistent with increased GnRH/gonadotropin release [30, 61, 62]. However, our current tSEM analyses are not specific to GnRH terminals as we have been unable to date to successfully optimize use of a GnRH monoclonal antibody in our monkey tissues. To address this, we used data available on GnRH immunofluorescence in the ME of the same pool of monkeys [29], and found no effects of age or treatment, although there was a trend for the E_2 + P_4 monkeys to have higher GnRH puncta density. It is generally thought that GnRH peptide content in the pericapillary region does not change with age in rodents [16, 63, 64], similar to our finding in these monkeys. However, another study from our lab found that there was an increase in GnRH immunoreactivity in the external zone of the ME in naturally aging intact rats [65], compared to no changes in ovariectomized aging rats [16], with differences potentially attributable to OVX status and/or the differing hormonal milieus. Future cytoarchitectural studies on GnRH terminals in the ME will add important insights into the nature and specificity of age- and hormone-regulated changes.

Effects of hormone were also noted in our study. The size of large neuroterminals in aged vehicle treated monkeys was greater than in the aged E_2 treated, and to a lesser extent the E_2 + P_4 group, which may indicate that the absence of hormones disrupted release mechanisms and/or the motility of the terminals, or that hormone treatment partially reversed effects of aging. When comparing the patterns in the distribution of terminal sizes in the different groups, we noticed that the vehicle and E_2 + P_4 groups had similar distribution patterns in both ages, and the E_2 groups were more similar to each other than to the other treatment groups within an age category. This may mean that the effects of E_2 are stronger than those of age on terminal size, but this is a purely qualitative observation that requires further experimentation to confirm.

Although there is a well-established morphological interactions between tanycytes and neuroterminals that is very dynamic in the pericapillary region of the ME, especially in response to hormones, there is a dearth of knowledge on age-related changes in the morphology of tanycytes [16, 17, 23, 24, 59, 60]. We found a significant age-related increase in the size of all glia, along with an age-related increase in the density and tissue fraction of large glia. E_2 treatment reversed the age-related increase in the glial tissue fraction. In fact,

the effects of age and hormones on large glial tissue fraction was particularly interesting, as the aged vehicle monkeys had significantly higher levels than the aged-E_2 and the young-vehicle monkeys, and suggesting that effects of age were mitigated by hormone treatment. It is well established that glia, including tanycytes, express a variety of estrogen receptors, and cultured rodent tanycytes have been shown to rapidly retract their processes when exposed to E_2 [19, 26, 27, 66, 67]. The neural-glial interactions, and hormone regulation, involve a number of factors including semaphorin 3A signaling via neuropilin-1 (Nrp-1; [25]), semaphoring 7A and its receptors PlexinC1 and Itgb1 [26], and other neurotropic factors and neurotransmitters. In the current monkey study, the increased size and percent of tissue occupied by glia observed in the aged relative to the young vehicle animals may be due to the combination of aging and a lack of the estradiol-triggered withdrawal signal, or a compensatory mechanism for the absence of estradiol.

Age and hormone effects on mitochondria in the ME

To our knowledge, this is the first study to demonstrate a change in the size of mitochondria in the ME with estradiol treatment, with a decrease occurring in AE compared to AV aged monkeys, but no differences in the young monkeys. Progesterone also reversed the effects of E_2 on mitochondrial size. In comparing these results to rodents, no age- or hormone-related alterations in mitochondria size were found in GnRH terminals or perikarya of rats [16, 58]. However, it is important to note that beyond the species differences, our work in rats was limited to a single cell type (GnRH terminals) whereas our monkey work did not differentiate among neuroterminal phenotypes at the EM level. In additional to their critical role in the synthesis of E_2 and other steroid hormones, hypothalamic mitochondria express estrogen receptors and therefore are directly responsive to E_2 [68–70]. The size and number of mitochondria correlate with the local energy demands, and degenerating mitochondria swell before decomposing [71]. Therefore, differences in mitochondrial size or numbers may represent altered cellular metabolism and/or dysfunction.

Other studies suggest that mitochondria are important targets for age- and/or hormone regulation. Hara et al. reported that while there were no changes in the density or size of mitochondria in the dorsolateral prefrontal cortex, there were morphological differences that correlated with behavioral outcomes [39]. Specifically, presynaptic donut-shaped mitochondria were in a much higher percentage of boutons in the aged OVX animals relative to young intact monkeys; this effect with aging was reversed by cyclic E_2 treatment [16, 58]. There is evidence that changes in mitochondrial structural and functional properties may underlie part of the brain's increased vulnerability to oxidative stress and other insults, and that E2 is protective against these changes [72–74]. Thus, mitochondria are important targets for future work, and region-specific differences in their properties may contribute to differential vulnerability of brain nuclei to age-related perturbations and E_2's ability to be neuroprotective.

Implications, Clinical Relevance, and Future Directions

Because the ME is the common site of convergence of all hypothalamic releasing- and inhibiting-hormones, morphological changes could affect a broad range of neuroendocrine functions such as reproduction, stress, growth, and metabolism. The endpoints in the ME

that were most affected by aging were the largest subsets of neuroterminals and glia, all increased in aged compared to young adult monkeys. There were more effects of hormones and their interactions with age, as E_2 decreased terminal size and tissue fraction, glial tissue fraction, and mitochondrial size in aged monkeys, effects that were with only two exception (tissue fraction of large neuroterminals, and mitochondrial size in nerve terminals) not seen in the young monkeys. These, while we did not observe gross morphological differences in any of the measured endpoints, these specific age- and hormone-changes may have functional implications. In addition, in comparison to other brain regions it appears that the phenotype of the monkey ME and other hypothalamic regions appears relatively resilient, making this a region of interest for comparison for brain regions that are more vulnerable to age-related changes.

Our monkey model has both strengths and limitations. Because our monkeys were OVX, they best approximate the human condition of surgical menopause. The fact that the ages of our animals roughly corresponded to young adult and middle-aged adult women is potentially useful for differentiating how age at oophorectomy affects neurobiological outcomes. We also find it interesting that more effects of E_2 treatment on properties of the ME were observed in aged monkeys, and that the directionality of effects was often to make the aged more like the young monkeys. Other clinical relevance comes from the conservation of menstrual cycle properties and the menopausal process itself in female rhesus macaques and women. While the functional importance of cytoarchitectural changes in the ME with age and hormones is not understood, a better understanding of how specific regions of the brain age, and effects of translationally-relevant hormone replacement therapies, is needed for the development of hormone treatments that may be targeted to neurological changes during menopause.

Acknowledgments

Grant support: NIH PO1 AG016765.

We are grateful to Dr. Jeffrey Roberts and Mary Roberts at the California National Primate Research Center for expert care of the animals. Dwight Romanovicz and John Mendenhall provided expert advice with electron microscopy use.

References

1. Harlow SD, Gass M, Hall JE, Lobo R, Maki P, Rebar RW, Sherman S, Sluss PM, de Villiers TJ. Executive summary of the Stages of Reproductive Aging Workshop + 10: addressing the unfinished agenda of staging reproductive aging. J Clin Endocrinol Metab. 2012; 97:1159–1168. [PubMed: 22344196]
2. Hall JE. Neuroendocrine physiology of the early and late menopause. Endocrinol Metab Clin North Am. 2004; 33:637–659. [PubMed: 15501638]
3. McEwen BS, Alves SE. Estrogen actions in the central nervous system. Endocrine Rev. 1999; 20:279–307. [PubMed: 10368772]
4. Avis NE, Brambilla D, McKinlay SM, Vass K. A longitudinal analysis of the association between menopause and depression. Results from the Massachusetts Women's Health Study. Ann Epidemiol. 1994; 4:214–220. [PubMed: 8055122]
5. Mansfield PK, Voda AM. Woman-centered information on menopause for health care providers: findings from the Midlife Women's Health Survey. Health Care Women Int. 1997; 18:55–72. [PubMed: 9119783]

6. Cauley JA, Robbins J, Chen Z, Cummings SR, Jackson RD, LaCroix AZ, LeBoff M, Lewis CE, McGowan J, Neuner J, Pettinger M, Stefanick ML, Wactawski-Wende J, Watts NB. Effects of estrogen plus progestin on risk of fracture and bone mineral density: the Women's Health Initiative randomized trial. JAMA. 2003; 290:1729–1738. [PubMed: 14519707]
7. Maki PM. Critical window hypothesis of hormone therapy and cognition: a scientific update on clinical studies. Menopause. 2013; 20:695–709. [PubMed: 23715379]
8. Rodriguez EM, Blazquez JL, Guerra M. The design of barriers in the hypothalamus allows the median eminence and the arcuate nucleus to enjoy private milieus: the former opens to the portal blood and the latter to the cerebrospinal fluid. Peptides. 2010; 31:757–776. [PubMed: 20093161]
9. Rodriguez EM, Blazquez JL, Pastor FE, Pelaez B, Pena P, Peruzzo B, Amat P. Hypothalamic tanycytes: a key component of brain-endocrine interaction. Int Rev Cytol. 2005; 247:89–164. [PubMed: 16344112]
10. Langlet F, Mullier A, Bouret SG, Prevot V, Dehouck B. Tanycyte-like cells form a blood-cerebrospinal fluid barrier in the circumventricular organs of the mouse brain. J Comp Neurol. 2013; 521:3389–3405. [PubMed: 23649873]
11. Prevot V, Bellefontaine N, Baroncini M, Sharif A, Hanchate NK, Parkash J, Campagne C, de Seranno S. Gonadotrophin-releasing hormone nerve terminals, tanycytes and neurohaemal junction remodelling in the adult median eminence: functional consequences for reproduction and dynamic role of vascular endothelial cells. J Neuroendocrinol. 2010; 22:639–649. [PubMed: 20492366]
12. Rangaraju NS, Xu JF, Harris RB. Pro-gonadotropin-releasing hormone protein is processed within hypothalamic neurosecretory granules. Neuroendocrinol. 1991; 53:20–28.
13. King JC, Tobet SA, Snavely FL, Arimura AA. LHRH immunopositive cells and their projections to the median eminence and organum vasculosum of the lamina terminalis. J Comp Neurol. 1982; 209:287–300. [PubMed: 6752217]
14. Yin W, Gore AC. The hypothalamic median eminence and its role in reproductive aging. Ann NY Acad Sci. 2010; 1204:113–122. [PubMed: 20738281]
15. Durrant AR, Plant TM. A study of the gonadotropin releasing hormone neuronal network in the median eminence of the rhesus monkey (Macaca mulatta) using a post-embedding immunolabelling procedure. J Neuroendocrinology. 1999; 11:813–821. [PubMed: 10520131]
16. Yin W, Wu D, Noel ML, Gore AC. Gonadotropin-releasing hormone neuroterminals and their microenvironment in the median eminence: effects of aging and estradiol treatment. Endocrinology. 2009; 150:5498–5508. [PubMed: 19819960]
17. Yin W, Mendenhall JM, Monita M, Gore AC. Three-dimensional properties of GnRH neuroterminals in the median eminence of young and old rats. The Journal of comparative neurology. 2009; 517:284–295. [PubMed: 19757493]
18. Prevot V. Glial-neuronal-endothelial interactions are involved in the control of GnRH secretion. J Neuroendocrinol. 2002; 14:247–255. [PubMed: 11999726]
19. de Seranno S, d'Anglemont de Tassigny X, Estrella C, Loyens A, Kasparov S, Leroy D, Ojeda SR, Beauvillain JC, Prevot V. Role of estradiol in the dynamic control of tanycyte plasticity mediated by vascular endothelial cells in the median eminence. Endocrinology. 2010; 151:1760–1772. [PubMed: 20133455]
20. Zoli M, Ferraguti F, Frasoldati A, Biagini G, Agnati LF. Age-related alterations in tanycytes of the mediobasal hypothalamus of the male rat. Neurobiol Aging. 1995; 16:77–83. [PubMed: 7723939]
21. Flament-Durand J, Brion JP. Tanycytes: morphology and functions: A review. Int Rev Cytol. 1985; 96:121–155. [PubMed: 2416706]
22. Akmayev IG, Fidelina OV. Tanycytes and their relation to the hypophyseal gonadotrophic function. Brain Res. 1981; 210:253–260. [PubMed: 6784884]
23. Baroncini M, Allet C, Leroy D, Beauvillain JC, Francke JP, Prevot V. Morphological evidence for direct interaction between gonadotrophin-releasing hormone neurones and astroglial cells in the human hypothalamus. J Neuroendocrinol. 2007; 19:691–702. [PubMed: 17680884]
24. Ojeda SR, Lomniczi A, Sandau US. Glial-gonadotrophin hormone (GnRH) neurone interactions in the median eminence and the control of GnRH secretion. J Neuroendocrinol. 2008; 20:732–742. [PubMed: 18601696]

25. Giacobini P, Parkash J, Campagne C, Messina A, Casoni F, Vanacker C, Langlet F, Hobo B, Cagnoni G, Gallet S, Hanchate NK, Mazur D, Taniguchi M, Mazzone M, Verhaagen J, Ciofi P, Bouret SG, Tamagnone L, Prevot V. Brain endothelial cells control fertility through ovarian-steroid-dependent release of semaphorin 3A. PLoS Biol. 2014; 12:e1001808. [PubMed: 24618750]

26. Parkash J, Messina A, Langlet F, Cimino I, Loyens A, Mazur D, Gallet S, Balland E, Malone SA, Pralong F, Cagnoni G, Schellino R, De Marchis S, Mazzone M, Pasterkamp RJ, Tamagnone L, Prevot V, Giacobini P. Semaphorin7A regulates neuroglial plasticity in the adult hypothalamic median eminence. Nat Commun. 2015; 6:6385. [PubMed: 25721933]

27. Micevych P, Bondar G, Kuo J. Estrogen actions on neuroendocrine glia. Neuroendocrinology. 2010; 91:211–222. [PubMed: 20332598]

28. Eghlidi DH, Haley GE, Noriega NC, Kohama SG, Urbanski HF. Influence of age and 17beta-estradiol on kisspeptin, neurokinin B, and prodynorphin gene expression in the arcuate-median eminence of female rhesus macaques. Endocrinology. 2010; 151:3783–3794. [PubMed: 20519367]

29. Naugle MM, Gore AC. GnRH neurons of young and aged female rhesus monkeys co-express GPER but are unaffected by long-term hormone replacement. Neuroendocrinology. 2014; 100:334–346. [PubMed: 25428637]

30. Gore AC, Windsor-Engnell BM, Terasawa E. Menopausal increases in pulsatile gonadotropin-releasing hormone release in a nonhuman primate (Macaca mulatta). Endocrinology. 2004; 145:4653–4659. [PubMed: 15231708]

31. Rubin BS, Bridges RS. Alterations in luteinizing hormone-releasing hormone release from the mediobasal hypothalamus of ovariectomized, steroid-primed middle-aged rats as measured by push-pull perfusion. Neuroendocrinology. 1989; 49:225–232. [PubMed: 2654689]

32. Wise PM, Dueker E, Wuttke W. Age-related alterations in pulsatile luteinizing hormone release: effects of long-term ovariectomy, repeated pregnancies and naloxone. Biol Reprod. 1988; 39:1060–1066. [PubMed: 3219379]

33. Scarbrough K, Wise PM. Age-related changes in pulsatile luteinizing hormone release precede the transition to estrous acyclicity and depend upon estrous cycle history. Endocrinology. 1990; 126:884–890. [PubMed: 2404750]

34. Gilardi KV, Shiderler SE, Valverde CR, Roberts JA, Lasley BL. Characterization of the onset of menopause in the rhesus macaque. Biol Reprod. 1997; 57:335–340. [PubMed: 9241047]

35. Bachevalier J, Landis LS, Walker LC, Brickson M, Mishkin M, Price DL, Cork LC. Aged monkeys exhibit behavioral deficits indicative of widespread cerebral dysfunction. Neurobiol Aging. 1991; 12:99–111. [PubMed: 2052134]

36. Hao J, Janssen WGM, Tang Y, Roberts JA, McKay H, Lasley B, Allen PB, Greengard P, Rapp PR, Kordower JH, Hof PR, Morrison JH. Estrogen increases the number of spinophilin-immunoreactive spines in the hippocampus of young and aged female rhesus monkeys. J Comp Neurol. 2003; 465:540–550. [PubMed: 12975814]

37. Hao J, Rapp PR, Janssen WG, Lou W, Lasley BL, Hof PR, Morrison JH. Interactive effects of age and estrogen on cognition and pyramidal neurons in monkey prefrontal cortex. Proc Natl Acad Sci U S A. 2007; 104:11465–11470. [PubMed: 17592140]

38. Hao J, Rapp PR, Leffler AE, Leffler SR, Janssen WG, Lou W, McKay H, Roberts JA, Wearne SL, Hof PR, Morrison JH. Estrogen alters spine number and morphology in prefrontal cortex of aged female rhesus monkeys. J Neurosci. 2006; 26:2571–2578. [PubMed: 16510735]

39. Hara Y, Yuk F, Puri R, Janssen WG, Rapp PR, Morrison JH. Presynaptic mitochondrial morphology in monkey prefrontal cortex correlates with working memory and is improved with estrogen treatment. Proc Natl Acad Sci U S A. 2014; 111:486–491. [PubMed: 24297907]

40. Rapp PR, Morrison JH, Roberts JA. Cyclic estrogen replacement improves cognitive function in aged ovariectomized rhesus monkeys. J Neurosci. 2003; 23:5708–5714. [PubMed: 12843274]

41. Wang AC, Hara Y, Janssen WG, Rapp PR, Morrison JH. Synaptic estrogen receptor-alpha levels in prefrontal cortex in female rhesus monkeys and their correlation with cognitive performance. J Neurosci. 2010; 30:12770–12776. [PubMed: 20861381]

42. Young ME, Ohm DT, Janssen WG, Gee NA, Lasley BL, Morrison JH. Continuously delivered ovarian steroids do not alter dendritic spine density or morphology in macaque dorsolateral prefrontal cortical neurons. Neuroscience. 2013; 255:219–225. [PubMed: 24120552]
43. Baxter MG, Roberts MT, Gee NA, Lasley BL, Morrison JH, Rapp PR. Multiple clinically relevant hormone therapy regimens fail to improve cognitive function in aged ovariectomized rhesus monkeys. Neurobiol Aging. 2013; 34:1882–1890. [PubMed: 23369546]
44. Ohm DT, Bloss EB, Janssen WG, Dietz KC, Wadsworth S, Lou W, Gee NA, Lasley BL, Rapp PR, Morrison JH. Clinically relevant hormone treatments fail to induce spinogenesis in prefrontal cortex of aged female rhesus monkeys. J Neurosci. 2012; 32:11700–11705. [PubMed: 22915112]
45. Hara Y, Park CS, Janssen WG, Punsoni M, Rapp PR, Morrison JH. Synaptic characteristics of dentate gyrus axonal boutons and their relationships with aging, menopause, and memory in female rhesus monkeys. J Neurosci. 2011; 31:7737–7744. [PubMed: 21613486]
46. Adams MM, Shah RA, Janssen WGM, Morrison JH. Different modes of hippocampal plasticity in response to estrogen in young and aged female rats. Proc Natl Acad Sci USA. 2001; 98:8071–8076. [PubMed: 11427724]
47. Hjelle OP, Chaudhry FA, Ottersen OP. Antisera to glutathione: characterization and immunocyochemical application to the rat cerebellum. European Journal of Neuroscience. 1994; 6:79793–79804.
48. Van Lookeren Campagne M, Oestreicher BA, Van Der Krift TP, Gispen WH, Verkleij AJ. Freeze-substitution and Lowicryl HM20 embedding of fixed rat brain: suitability for immunogold ultrastructural localization of neural antigens. J Histochem Cytochem. 1991; 39:1267–1279. [PubMed: 1833448]
49. Chaudhry FA, Lehre KP, Campagne MVL, Ottersen OP, Danbolt NC, Storm-Mathisen J. Glutamate transporters in glial plasma membranes: highly differentiated localizations revealed by quantitative ultrastructural immunocytochemistry. Neuron. 1995; 15:711–720. [PubMed: 7546749]
50. Kuwajima M, Mendenhall JM, Harris KM. Large-volume reconstruction of brain tissue from high-resolution serial section images acquired by SEM-based scanning transmission electron microscopy. Methods Mol Biol. 2013; 950:253–273. [PubMed: 23086880]
51. Kuwajima M, Mendenhall JM, Lindsey LF, Harris KM. Automated transmission-mode scanning electron microscopy (tSEM) for large volume analysis at nanoscale resolution. PLoS One. 2013; 8:e59573. [PubMed: 23555711]
52. Schindelin J, Arganda-Carreras I, Frise E, Kaynig V, Longair M, Pietzsch T, Preibisch S, Rueden C, Saalfeld S, Schmid B, Tinevez JY, White DJ, Hartenstein V, Eliceiri K, Tomancak P, Cardona A. Fiji: an open-source platform for biological-image analysis. Nat Methods. 2012; 9:676–682. [PubMed: 22743772]
53. Peters, A.; Palay, SL.; Webster, H. The Fine Structure of the Nervous System. 3. New York: Oxford University Press; 1991.
54. Yin W, Sun Z, Mendenhall JM, Walker DM, Riha PD, Bezner KS, Gore AC. Expression of Vesicular Glutamate Transporter 2 (vGluT2) on Large Dense-Core Vesicles within GnRH Neuroterminals of Aging Female Rats. PLoS One. 2015; 10:e0129633. [PubMed: 26053743]
55. Urbanski HF. Monoclonal antibodies to luteinizing hormone-releasing hormone: Production, characterization and immunocytochemical application. Biol Reprod. 1991; 44:681–686. [PubMed: 2043738]
56. Hara Y, Punsoni M, Yuk F, Park CS, Janssen WG, Rapp PR, Morrison JH. Synaptic distributions of GluA2 and PKMzeta in the monkey dentate gyrus and their relationships with aging and memory. J Neurosci. 2012; 32:7336–7344. [PubMed: 22623679]
57. Anthony EL, King JC, Stopa EG. Immunocytochemical localization of LHRH in the median eminence, infundibular stalk, and neurohypohysis. Evidence for multiple sites of releasing hormone secretion in humans and other mammals. Cell Tissue Res. 1984; 236:5–14. [PubMed: 6370455]
58. Witkin JW, Romero MT. Comparison of ultrastructural characteristics of gonadotropin-releasing hormone neurons in prepubertal and adult male rats. Neuroscience. 1995; 64:1145–1151. [PubMed: 7753381]

59. Prevot V, Dutoit S, Croix D, Tramu G, Beauvillain JC. Semi-quantitative ultrastructural analysis of the localization and neuropeptide content of gonadotropin releasing hormone nerve terminals in the median eminence throughout the estrous cycle of the rat. Neuroscience. 1998; 84:177–191. [PubMed: 9522372]
60. Prevot V, Croix D, Bouret S, Dutoit S, Tramu G, Stefano GB, Beauvillain JC. Definitive evidence for the existence of morphological plasticity in the external zone of the median eminence during the rat estrous cycle: implication of neuro-glio-endothelial interactions in gonadotropin-releasing hormone release. Neuroscience. 1999; 94:809–819. [PubMed: 10579572]
61. Park SJ, Goldsmith LT, Weiss G. Age-related changes in the regulation of luteinizing hormone secretion by estrogen in women. Exp Biol Med. 2002; 227:455–464.
62. Gill S, Sharpless JL, Rado K, Hall JE. Evidence that GnRH decreases with gonadal steroid feedback but increases with age in postmenopausal women. J Clin Endocrinol Metab. 2002; 87:2290–2296. [PubMed: 11994378]
63. Rubin BS, King JC, Bridges RS. Immunoreactive forms of luteinizing hormone-releasing hormone in the brains of aging rats exhibiting persistent vaginal estrus. Biol Reprod. 1984; 31:343–351. [PubMed: 6383488]
64. Bestetti GE, Reymond MJ, Blanc F, Boujon CE, Furrer B, Rossi GL. Functional and morphological changes in the hypothalamopituitary-gonadal axis of aged female rats. Biol Reprod. 1991; 45:221–228. [PubMed: 1786286]
65. Kermath BA, Riha PD, Sajjad A, Gore AC. Effects of chronic NMDA-NR2b inhibition in the median eminence of the reproductive senescent female rat. Journal of neuroendocrinology. 2013; 25:887–897. [PubMed: 23957788]
66. Almey A, Filardo EJ, Milner TA, Brake WG. Estrogen receptors are found in glia and at extranuclear neuronal sites in the dorsal striatum of female rats: evidence for cholinergic but not dopaminergic colocalization. Endocrinology. 2012; 153:5373–5383. [PubMed: 22919059]
67. Fuente-Martin E, Garcia-Caceres C, Morselli E, Clegg DJ, Chowen JA, Finan B, Brinton RD, Tschop MH. Estrogen, astrocytes and the neuroendocrine control of metabolism. Rev Endocr Metab Disord. 2013; 14:331–338. [PubMed: 24009071]
68. Alvarez-Delgado C, Mendoza-Rodriguez CA, Picazo O, Cerbon M. Different expression of alpha and beta mitochondrial estrogen receptors in the aging rat brain: interaction with respiratory complex V. Exp Gerontol. 2010; 45:580–585. [PubMed: 20096765]
69. Baulieu EE, Robel P. Neurosteroids: a new brain function? J Steroid Biochem Mol Biol. 1990; 37:395–403. [PubMed: 2257243]
70. Woolley CS. Acute effects of estrogen on neuronal physiology. Annu Rev Pharmacol Toxicol. 2007; 47:657–680. [PubMed: 16918306]
71. Fiala JC, Feinberg M, Peters A, Barbas H. Mitochondrial degeneration in dystrophic neurites of senile plaques may lead to extracellular deposition of fine filaments. Brain Struct Funct. 2007; 212:195–207. [PubMed: 17717688]
72. Simpkins JW, Yi KD, Yang SH, Dykens JA. Mitochondrial mechanisms of estrogen neuroprotection. Biochim Biophys Acta. 2010; 1800:1113–1120. [PubMed: 19931595]
73. Rettberg JR, Yao J, Brinton RD. Estrogen: a master regulator of bioenergetic systems in the brain and body. Front Neuroendocrinol. 2014; 35:8–30. [PubMed: 23994581]
74. Shi C, Xu J. Increased vulnerability of brain to estrogen withdrawal-induced mitochondrial dysfunction with aging. J Bioenerg Biomembr. 2008; 40:625–630. [PubMed: 19139976]

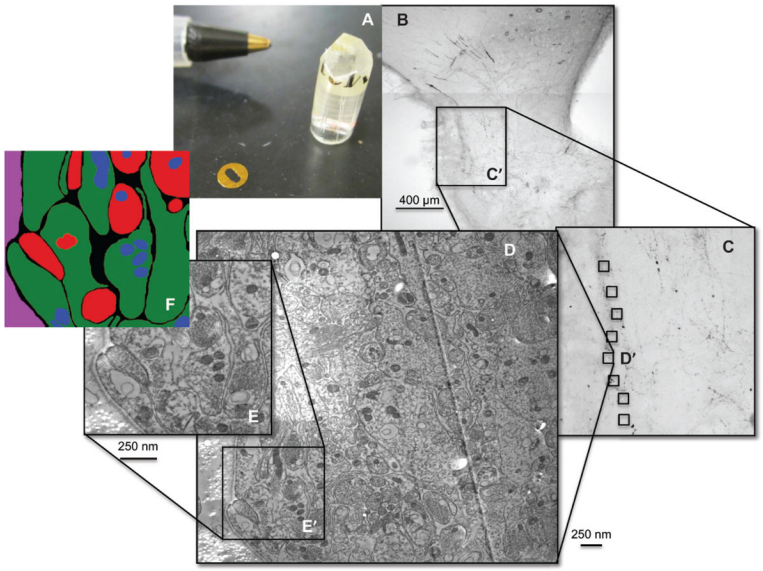

Figure 1.

The sample preparation is illustrated. In (A), the dissected ME is shown embedded in the lowicryl resin, next to a formvar-coated gold slot grid and with a pen in the background for perspective. In (B), a representative section was immunolabeled with GnRH (black cells and fibers) to visualize the area of the ME located in close proximity to the portal vasculature, shown to illustrate the region that was selected for the embedding procedure. An area corresponding to the inset (C′) corresponds to the region shown at greater magnification in panel C. This region was dissected, prepared, and mounted in a lowicryl block, and ultrathin sections were collected near 10 capillaries along the basal lamina. The area labeled D′ in panel C is shown at higher magnification in (D), which is a wide-field tSEM image. Within this region, 5 μm^2 subregions were segmented into the cellular components (E and F) used for subsequent analyses.

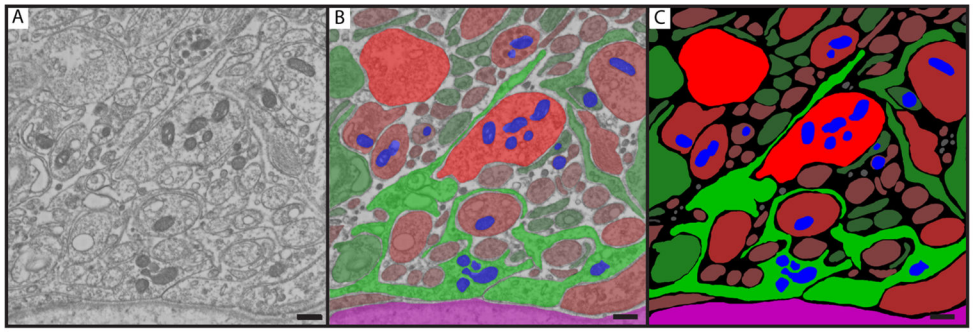

Figure 2.

The image segmentation process is demonstrated for a representative AV monkey, with the raw image (A), the final segmented image (C), and an overlay of the two (B) shown. The red areas are neuroterminals, green is glia, blue is mitochondria, and magenta is the portal capillary bed at the bottom of the image. The relative intensity of the color corresponds to the size class to which each object is assigned, with the larger objects more brightly colored and smaller objects more darkly colored. Scale bar = 400 nm.

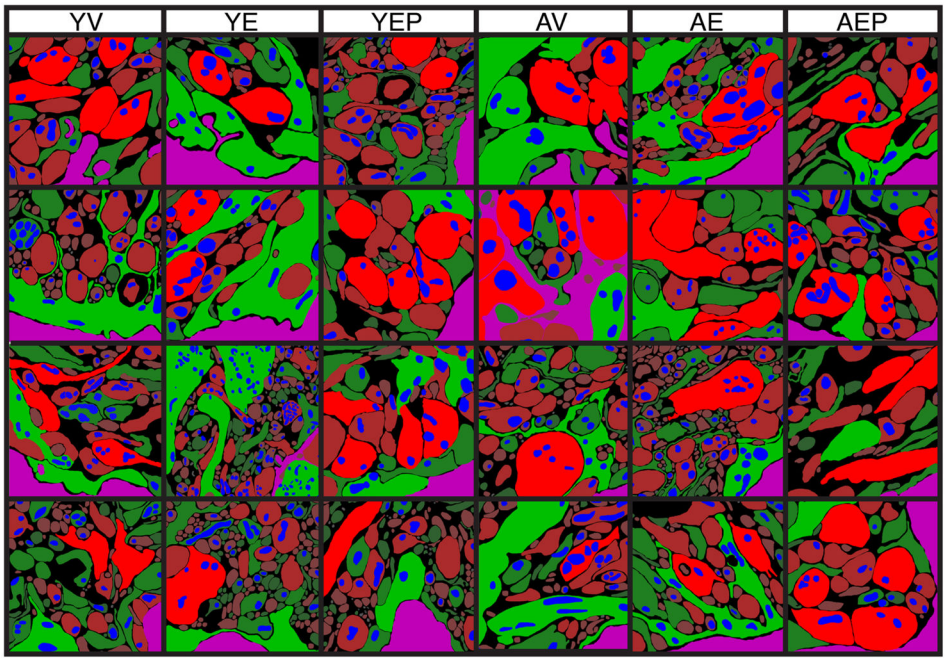

Figure 3.

Representative micrographs of the ultrastructural organization of the ME are shown for 4 monkeys from each of the 6 groups. Red=neuroterminals, green=glia, blue=mitochondria, and magenta=portal capillary bed, the latter always positioned at the lower/righthand sides of the images. The relative intensity of the color corresponds to the size class to which each object is assigned, with the larger objects more brightly colored and smaller objects more darkly colored. Scale bar = 400 nm.

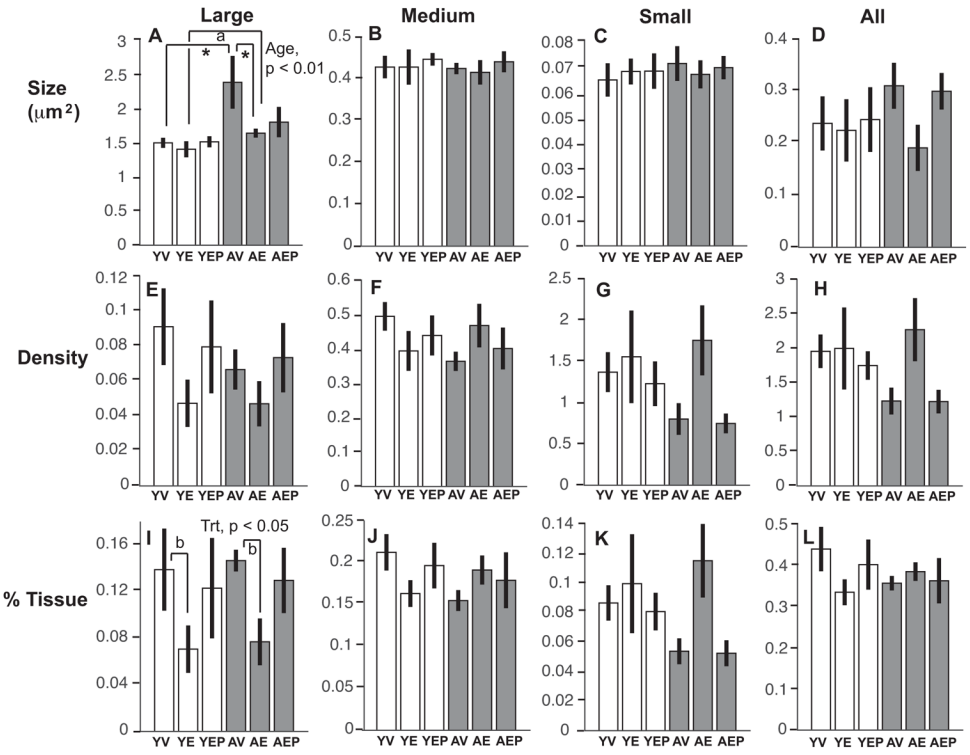

Figure 4.

Neuroterminal size (A–D), density (number of cells per μm^2, E–H), and area fraction (% tissue represented by each terminal type, I–L), are shown for large, medium, small, and all terminals (mean ± SEM) from left to right. There were significant effects of age on the average size of the large terminals, and an age by treatment interaction (panel A, $p<0.01$; *$p < 0.05$ AV vs. AE, and AV vs. YV; $^{a}p < 0.05$ YE vs. AE). A treatment effect and an age by treatment interaction were found for the % tissue, driven by E2 monkeys of both ages having a smaller tissue fraction compared to age-matched vehicle counterparts (panel I, $^{b}p < 0.05$ YV vs. YE, and AV vs. AE). Abbreviation: Trt, Treatment.

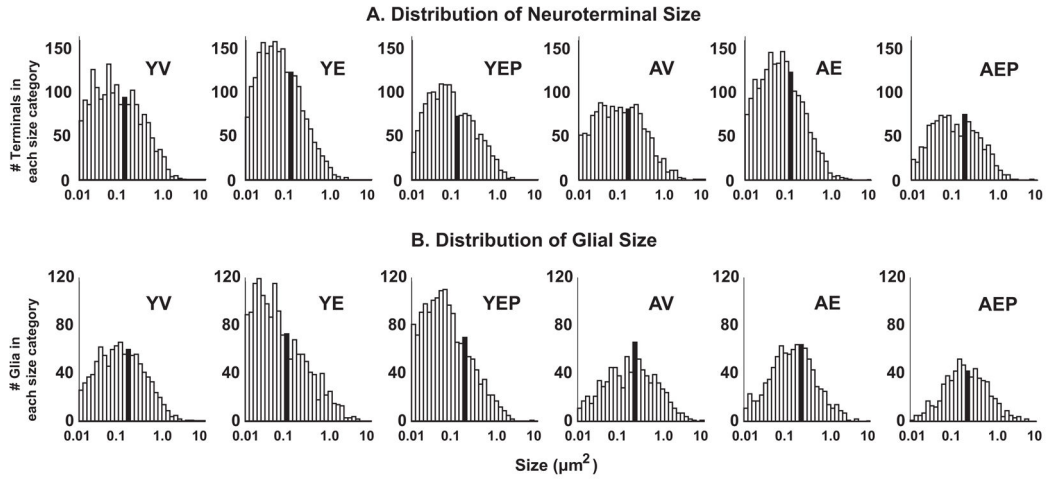

Figure 5.

The distribution of the size of neuroterminals (A) and glia (B) is shown for each of the 6 groups. The number of terminals is on the y-axis, and the size (μm^2) on the x-axis is plotted on a logarithmic scale. The median value for each group is indicated with the solid black bars.

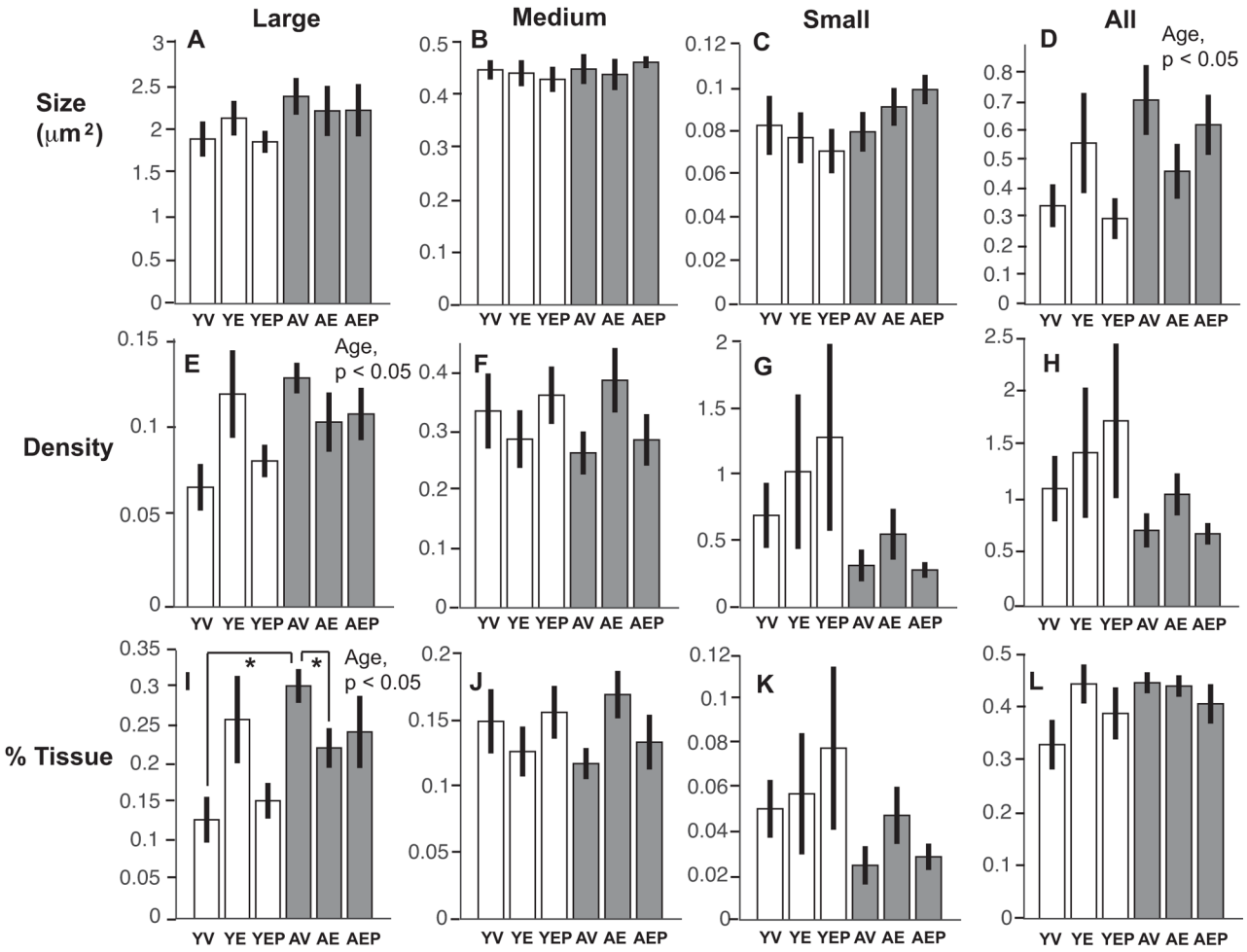

Figure 6.

Glial size (A–D), density (E–H), and area fraction (% tissue represented by each glial type, I–L) are shown for large, medium, small, and all glia (mean ± SEM) from left to right.. There was a significant effect of age on the average size of all glia, and on the density of large glia ($p<0.05$ for both; aged>young). The large glial tissue fraction was greater in aged than young monkeys ($p<0.05$), and a significant interaction effect was found that was driven by AV having higher levels than both YV and AE (panel I, *$p<0.05$ for both).

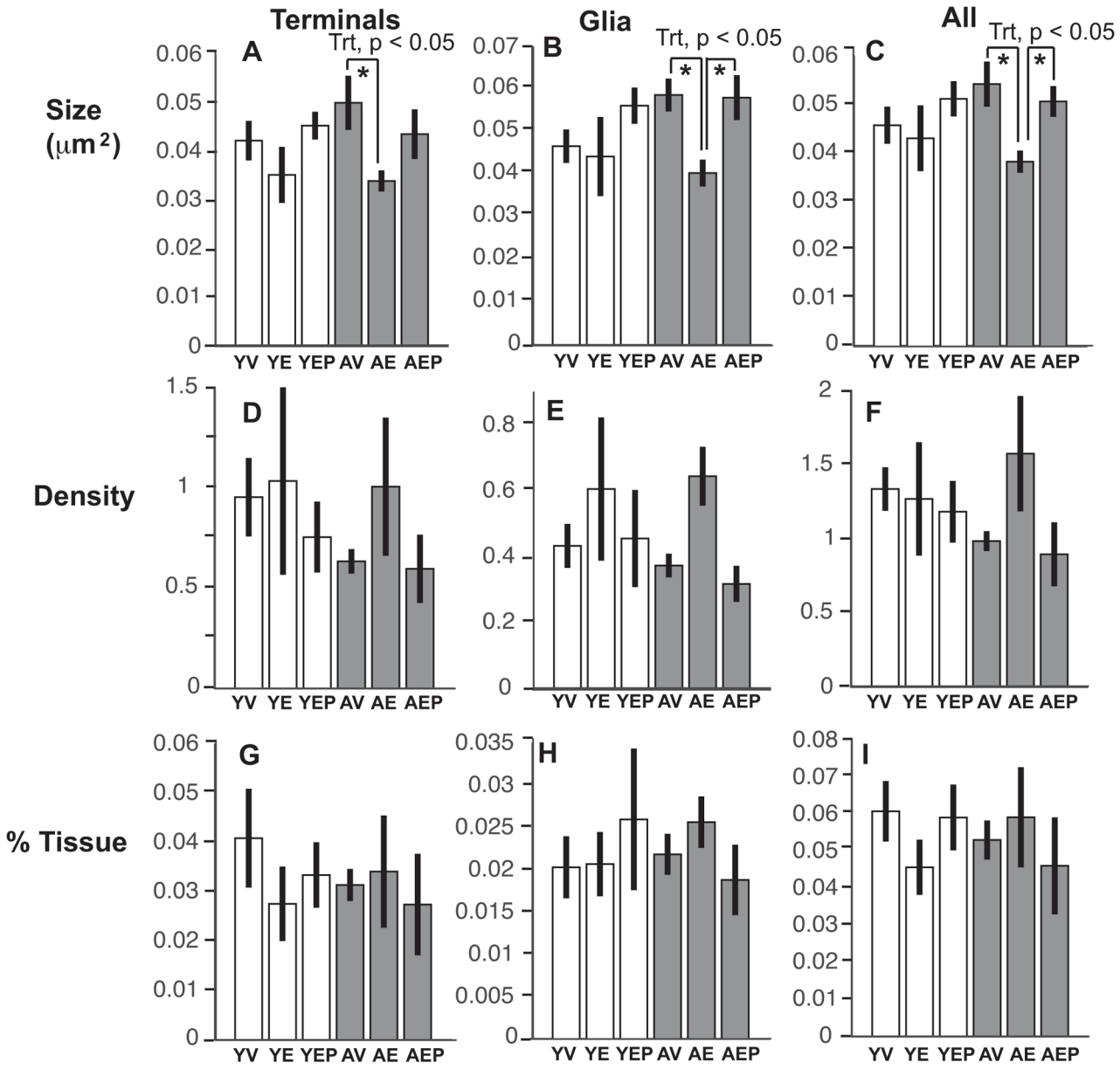

Figure 7.

Mean mitochondrial size (A–C), density (D–F), and area fraction (G–I) are shown (mean ± SEM). There were significant effects of treatment on the size of mitochondria in nerve terminals, in glia, and in both combined (*p<0.05 for all). This was driven by the E_2 groups having smaller mitochondrial sizes than vehicle groups, with AE<AV for all categories, and AE<AEP for all mitochondria and glial mitochondria. For glial mitochondria, the age by treatment analysis revealed a trend for AV>YV (p=0.07). Mitochondrial density and tissue fraction were unaffected by age or treatment. Abbreviation: Trt, Treatment.

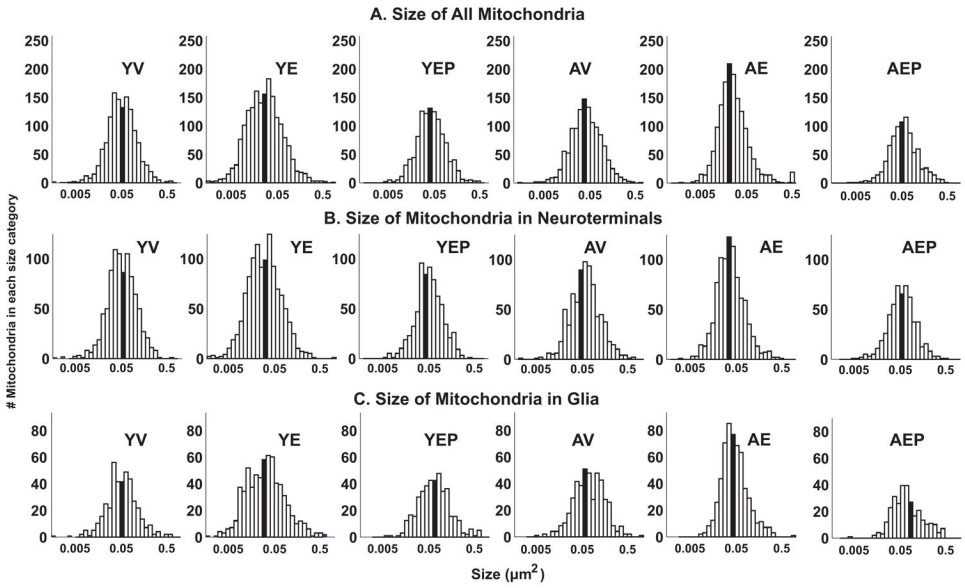

Figure 8.

The distribution of the size of mitochondria is shown for each of the 6 groups. The number of mitochondria is on the y-axis and the size (μm^2) is plotted on a logarithmic scale on the x-axis. The median value for each group is indicated with the solid black bars.

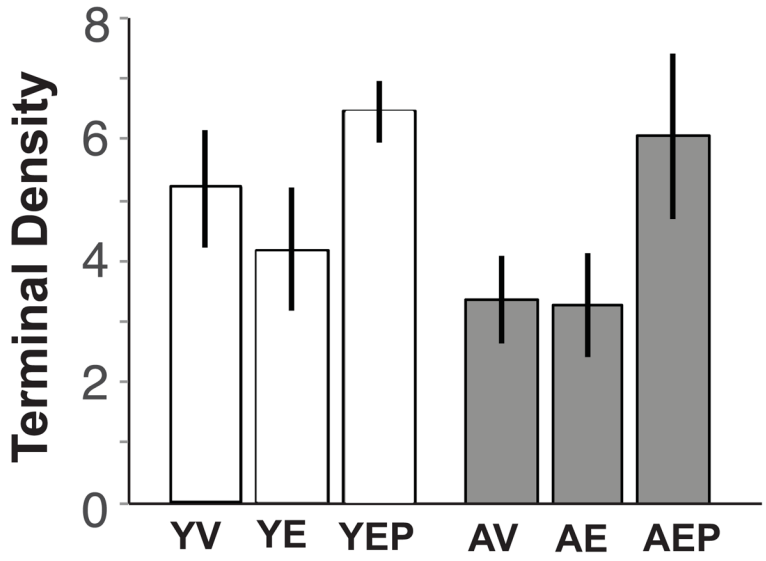

Figure 9.

The density of GnRH immunoreactive puncta in the external ME was determined by immunofluorescence and confocal microscopy. GnRH density was not significantly affected by age, treatment, or their interactions, although there was a trend ($p = 0.097$) for a treatment effect attributable to the $E_2 + P_4$ groups having non-significantly higher density than the vehicle or E_2-alone groups.

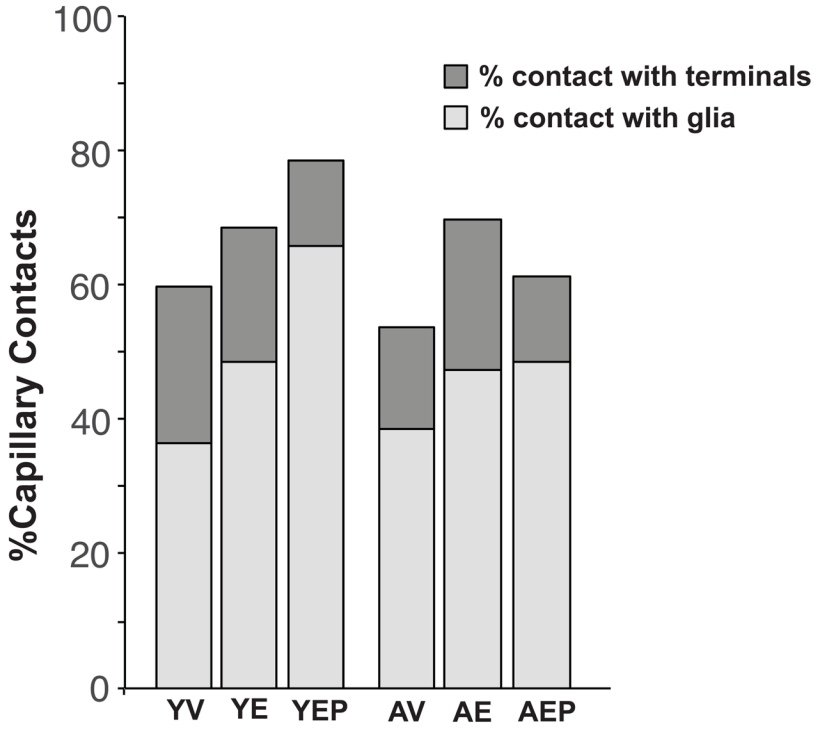

Figure 10.

The percentage of contacts between capillaries and terminals (dark gray) and glia (light gray) is shown for the 6 groups of monkeys.